

Optimal Sampling and Principal Component Selections for Spectral Image Browsing

Juha Lehtonen[^], Jussi Parkkinen and Markku Hauta-Kasari

Department of Computer Science and Statistics, University of Joensuu, P.O. Box 111, FI-80101 Joensuu, Finland

E-mail: juha.lehtonen@cs.joensuu.fi

Timo Jaaskelainen

Department of Physics and Mathematics, University of Joensuu, P.O. Box 111, FI-80101 Joensuu, Finland

Abstract. Spectral imaging is becoming popular. Spectral accuracy in measurements is an important factor, especially now when fluorescent and light emitting diode (LED) based light sources are becoming common. Browsing image sets in a modern network is also becoming relevant, but the problem with spectral data is that the file sizes are so large. An efficient compression method suitable for browsing purposes consists of principal component analysis with spatial subsampling. In this study, the optimal combinations of a sampling interval and parameters of the developed compression method are found for different data sets under several light sources. It is shown that depending on the light source, 3–20 nm sampling intervals are required. In addition, with different light sources and data sets, between three and six principal components must be used. With a suitable spatial subsampling mask, high compression ratios can be achieved with good results. The spatial subsampling is a fast operation and can be done online before transmission, which gives the client user a possibility to choose the compression ratio.
© 2009 Society for Imaging Science and Technology.
[DOI: 10.2352/J.ImagingSci.Technol.2009.53.6.060503]

INTRODUCTION

Color is usually represented in a three-dimensional space, such as in a RGB space. However, ordinary trichromatic representations of color have been shown to be problematic: one cannot describe color accurately enough, there is metamerism,¹ and three-dimensional color coordinations are device dependent.² Therefore, the full spectrum of a color is needed to avoid these problems. Several examples exist that describe the needs of spectral imaging. Different applications are found in telemedicine,³ quality control,⁴ e.g., in plastics, wood and paper industries, digital museums,⁵ and also in e-commerce in items where color is meaningful, such as in clothing, fine arts, or paints.

It is not possible to capture a full digital spectral image with a single shot. Commercial displays or printers are incapable of representing a spectral image on a computer screen as a picture or of printing it. The closest examples nowadays are six-primary color gamut based high definition television (HDTV) monitors⁶ and video cameras.⁷ Multiprimary printers producing color with more than four primaries have

also been developed.⁸ Still, different types of very sophisticated and accurate measuring devices have been developed for the saving of spectral images. These devices are spectral or spatial scanners based on different technologies, such as an acousto-optic tunable filter,⁹ liquid crystal tunable filter,¹⁰ spectral scanning with a grating,⁴ or interferometry.¹¹ Many spectral measurements are done with 10 nm or even wider sampling intervals because of the limitations of the measurement devices. However, it has been shown that, for example, a 10 nm sampling interval is not enough under fluorescent light sources.^{12,13} The sampling interval issue is becoming more and more important because of the increasing popularity of fluorescent and LED based illumination.

One problem in spectral images is that the raw format usually requires a large memory space, e.g., a 16-bit spectral image between a 380 and 780 nm range with a 5 nm interval and a spatial size of 1920×1080 pixels requires 320 MB. Therefore, one cannot save several images on a DVD or a USB memory stick. In addition, transferring the images through an ordinary network is very slow. Several compression methods have been developed to correct these problems. One proposal is a method compatible with standard trichromatic methods,¹⁴ where additional components are saved with some standard trichromatic information, and for which it was shown that four additional components were required to get all used 354 reflectance spectra of objects below $\Delta E < 3.0$. A method based on address-predictive vector quantization (VQ) has also been developed,¹⁵ where compression ratio (CR) of 40:1 and signal-to-noise ratio (SNR) of 23 dB can be achieved. Independent component analysis^{16,17} and principal component analysis (PCA)^{18–21} are also widely used, where the eigenimages are projections of the image formed by the eigenvectors. Parkkinen et al.¹⁸ used eight eigenvectors for the Munsell matte data set to obtain an average $\Delta E < 0.5$. Lim et al.²² found six components for SNR of 40 dB for 220-band airborne visible/infrared imaging spectrometer (AVIRIS) airborne images. Additionally, different methods are used to compress the eigenimages, for example standard JPEG based straightforward subsampling²³ or via discrete cosine transform (DCT).²⁴ With fast straightforward subsampling,²³ 40-band

[^]IS&T Member.

Received Oct. 29, 2008; accepted for publication Jul. 31, 2009; published online Oct. 12, 2009.

1062-3701/2009/53(6)/060503/10/\$20.00.

images of natural scenes were used, resulting in CR of 27:1. With the DCT method,²⁴ 16-band airborne multispectral images between 360 and 1210 nm were used, resulting in CR of 5:1 and 40:1 for a near lossless and visually lossless result, respectively. In addition, a discrete wavelet transform (DWT) familiar with JPEG2000 is used in Kaarna²⁵ and Du and Fowler.²⁶ A combination of DWT and gain shape VQ has been developed,²⁷ where SNR of 16–19 dB with CR of 40:1–10:1 and SNR of 12–20 dB with CR of 50:1–10:1 for 6-band LANDSAT satellite images and 14–19 bands of GER satellite images were achieved, respectively. Comparison between PCA, Fourier, and wavelet bases for reflectance representation and estimation was done by Mansouri et al.²⁰ A region-based eigensubspace transform added with JPEG is a method²⁸ that results in a peak signal-to-noise ratio (PSNR) near 30 dB with CR of 15:1 and 36:1. An adaptive recursive bidirection prediction is (RBP) with JPEG is also a method,²⁹ resulting in SNR of 39 dB with CR of 47:1 for 224-band AVIRIS airborne images. An adaptive PCA method,³⁰ which continuously adjusts the eigenvectors, results in PSNR of 26–30 dB with CR of 34:1–27:1 for 7-band satellite images. In addition, lossless methods are region-based³¹ and DWT based³² compression of PCA eigenimages, resulting in CR of 2.3:1 and 2.8–2.9:1 for 7-band satellite and 224-band airborne images, respectively. PCA and some nonlinear dimensional reduction techniques, such as Laplacian eigenmaps and isometric feature mapping were used by Carmona and Lenz²¹ for performance evaluation.

Since spectral imaging is expanding for several purposes,^{3–5} spectral image browsing via internet will also be needed. The client user should be able to browse several spectral images located in a server with an internet browser in an ordinary network. PCA is a very efficient way to reduce memory requirements. Also, straightforward spatial subsampling of the eigenimages is so fast operation that it can be done on uncompressed eigenimages online before transmitting the image to the user. Because of this, the user may adjust the final compression ratio and image accuracy by selecting from different subsampling masks. Hauta-Kasari et al.²³ proposed this method with reflectance spectral data for browsing purposes. By using this method, this study determines optimal selections for a sampling interval used in measuring, and the number of required principal components and suitable subsampling mask used in compression. The analysis is done with several modern data sets and for data under different light sources and illuminants. According to Lehtonen et al.¹² with a Munsell matte spectra set,³³ even a 20 nm sampling interval is sufficient for reflectance spectra, but 10 nm may not be adequate for peaky fluorescent light sources. The same conclusion was reached by Trussell and Kulkarni,¹³ i.e., a 10 nm sampling interval for illuminations with sharp spectral peaks. In this study, we expand the point color estimation to spectral images that include compression with PCA and spatial JPEG based subsampling.

THEORY

Let S^o be the original spectral image with a 1 nm sampling interval and with dimensions $m \times n \times w^o$, where m and n denote the height and width of the image and w^o denotes the number of channels in a spectral dimension. Let the spectral image with $\Delta\lambda$ nm sampling interval be S with dimensions $m \times n \times w$, where w denotes the number of channels in the spectral dimension $w \leq w^o$. To determine the best parameters, the original data are first converted to a $\Delta\lambda$ nm sampling interval from the original. This is straightforward, by taking the values of every $\Delta\lambda$ th wavelength from the measured image. The values in other wavelengths are removed.

Spectral Image Compression

The spectral image compression method used is based on PCA and JPEG based subsampling. Following the standard procedure in spectral image analysis, we use a correlation matrix instead of a covariance matrix in defining eigenvectors for color spectrum reconstruction. Let S^v be a vector-ordered $w \times mn$ dimensional representation of spectral image S , whose mn pixels are ordered as a vector. Let C be the correlation matrix

$$C = \sum_{i=1}^{mn} S_i^v S_i^{vT}, \quad (1)$$

where S_i^v is the i th spectrum of spectral image S^v and T means matrix transpose. Next, the h first eigenvectors ($h \leq w$) ordered by the largest eigenvalues can be calculated, which will form the eigenvectors $(\tau_1, \tau_2, \dots, \tau_h)$ of the spectral image, where τ_k is the k th eigenvector of the matrix C . The vector-ordered eigenimages P^v are then formed with the inner product

$$P^v = (\tau_1, \tau_2, \dots, \tau_h)^T S^v. \quad (2)$$

Let P denote the normal spectral image form of P^v with dimensions $m \times n \times h$. Let B_k also be a predefined mask matrix of predefined size $t_1 \times t_2$ for k th eigenimage, where

$$\sum_{i=1}^{t_1} \sum_{j=1}^{t_2} B_k(i, j) = 1. \quad (3)$$

This mask defines weights for calculating a weighted sum of a block in spatial subsampling, which will replace the block. The new subsampled eigenimages P^c are then

$$P_k^c(x_1, x_2) = \sum_{i=1}^{t_1} \sum_{j=1}^{t_2} [B_k(i, j) P_k(y_1, y_2)],$$

$$\text{with } y_1 = [(x_1 - 1)t_1 + i] \in [1, \dots, m],$$

$$y_2 = [(x_2 - 1)t_2 + j] \in [1, \dots, n],$$

$$x_1 = 1 \dots \left\lfloor \frac{m}{t_1} \right\rfloor, \quad x_2 = 1 \dots \left\lfloor \frac{n}{t_2} \right\rfloor, \quad k = 2, \dots, h, \quad (4)$$

where P_k is the k th $m \times n$ dimensional unsubsampled eigenimage and h is the number of eigenimages. The

subsampling phase is not applied for the first eigenimage. The final compressed spectral image is then a combination of the first eigenimage, other subsampled eigenimages, and eigenvectors. The subsampling is based on a known method of JPEG subsampling, where the image is calculated according to a YC_bC_r color coordinate system.³⁴ The Y component represents the achromatic information, while the other two components C_b and C_r represent the color information. The Y component is untouched while the other components are compressed with the mask. Similarly, while the first eigenimage is close to the achromatic data, one can apply this method to eigenimages.

Spectral Image Reconstruction

In the reconstruction, these two phases are conducted in reverse order by filling the block with the calculated pixel, which replaced it in compression. The unsampling phase is defined as

$$P_k^r(y_1, y_2) = P_k^c(x_1, x_2),$$

$$\text{with } y_1 = [(x_1 - 1)t_1 + i] \in [1, \dots, m],$$

$$y_2 = [(x_2 - 1)t_2 + j] \in [1, \dots, n],$$

$$x_1 = 1 \dots \left\lceil \frac{m}{t_1} \right\rceil, \quad x_2 = 1 \dots \left\lceil \frac{n}{t_2} \right\rceil, \quad k = 2, \dots, h,$$

$$\forall i = 1, \dots, t_1, \quad \forall j = 1, \dots, t_2, \quad (5)$$

where P_k^r is the k th reconstructed eigenimage, and $P_1^r = P_1$. The pixels of the eigenimages are reordered to a vector, thus, generating vector-formed eigenimages P^{vr} , which are used for the spectral image reconstruction, as follows:

$$S^{vr} = (\tau_1, \tau_2, \dots, \tau_h)^T P^{vr}. \quad (6)$$

This compression method can also be done in reverse order by first subsampling all channels in the original spectral image and then calculating the correlation matrix, eigenvectors, and eigenimages from the subset of pixels. This reverse algorithm arrives at the same result and is also computationally faster.²³ However, all channels must then have the same mask.

Quality and Error Measures

Let S^r be a representation of S^{vr} , where the pixels are reordered as in the original spectral image S^o . One error measure (ΔE) and two quality measures (PSNR, GFC) were used to compare the original spectral image S^o and reconstructed image S^r . The ΔE error is based on the properties of the human eye and is used as the error of visibility. The spectra are first converted to the CIE $L^*a^*b^*$ color space via an XYZ space using CIE 1931 color matching functions (2° standard observer). After this, the ΔE error is calculated as

$$\Delta E = (\Delta L^{*2} + \Delta a^{*2} + \Delta b^{*2})^{1/2}, \quad (7)$$

where ΔL^* , Δa^* , and Δb^* are the color coordinate differences between the original and reconstructed spectra in the CIE $L^*a^*b^*$ color space. Usually, average $\Delta E < 1.0$ is not visually discernable.³⁵ In this study, we used several spectral image sets under different light sources. Since the light source is already included in the data, equal-energy illuminant E was used to calculate the ΔE error. For the quality measures, the reconstructed image needs to be interpolated from the $\Delta \lambda$ nm interval to the original one, where Lagrange interpolation given by Fairman³⁶ was used. The quality measure PSNR is peak signal-to-noise ratio in decibels (dB) and it is defined as

$$\epsilon_{\text{PSNR}} = 10 \log_{10} \frac{\hat{s}^2}{\epsilon_{\text{MSE}}}, \quad (8)$$

where \hat{s} is the theoretical maximum of a channel value and ϵ_{MSE} is the mean square error. PSNR is widely used in image compression analysis. The GFC error is a correlation measure, defined as

$$\epsilon_{\text{GFC}} = \frac{\sum_{\lambda} s_{\lambda}^o s_{\lambda}^r}{\left[\sum_{\lambda} (s_{\lambda}^o)^2 \right]^{1/2} \left[\sum_{\lambda} (s_{\lambda}^r)^2 \right]^{1/2}}, \quad (9)$$

where s_{λ}^o and s_{λ}^r are channel values of the original and reconstructed spectrum from the λ nm wavelength, respectively. Hernández-Andrés et al.³⁷ defined this quality measure with a value of 0.995 as an accurate limit and 0.999 as a good limit. These quality measures are used to describe the mathematical difference of the original and reconstructed spectral image. All the symbols used in this study are listed in Table I.

TEST DATA

Five different spectral image sets were used in this research,^{33,38–40} described in more detail in Table II. In addition, five different real light sources shown in Figure 1 and five standard illuminants (A, D65, F2, F8, and F11) were used. All the images were computationally converted to be like the spectra that have been measured under the light sources. Different combinations between image sets and light sources generated a total of 55 different test sets, including image sets without a light source. This light source conversion simulates the result of spectral image measurement under the light source by assuming that the reflectance spectra are unknown.

All original spectral images contain 61 or 31 components, between 400 and 700 nm with a 5 nm or a 10 nm interval. Color distributions of different sets are shown in Figure 2 as (a^*, b^*) coordinate pairs projected from a CIE $L^*a^*b^*$ color space. The color conversion was done with CIE 1931 color matching functions (2° standard observer) and under a D65 illuminant. The darker the point is in the coordination, the more pixels with the same coordinate exist in the set. It can be seen that the colors vary greatly, especially

Table I. Symbols.

Symbol	Definition	Symbol	Definition
B_k	Mask for k th eigenimage	P^r	Reconstructed eigenimages
b_k^i	i th mask value for k th eigenimage	P_k^r	k th reconstructed eigenimage
C	Correlation matrix	P^v	Vector-ordered representation of P
ΔE	ΔE error measure	P^{vr}	Vector-ordered representation of P^r
$\Delta\lambda$	Sampling interval	S	Spectral image with $\Delta\lambda$ nm sampling interval
ε_{GFC}	GFC quality measure	S^o	Original spectral image
ε_{MSE}	Mean square error	S^r	Reconstructed spectral image
$\varepsilon_{\text{PSNR}}$	PSNR quality measure	S^v	Vector-ordered representation of S
h	Number of eigenvectors/eigenimages	s_j^r	j th spectrum of S^r
i, j	Counters for spatial directions	S^{vr}	Vector-ordered representation of S^r
k	Counter for eigenvectors/eigenimages	s_λ^o	Value of original spectrum in wavelength λ nm
λ	Wavelength counter (λ nm)	s_λ^r	Value of reconstructed spectrum in wavelength λ nm
m	Height of original spectral image	\hat{s}	Theoretical maximum of a channel value
n	Width of original spectral image	τ_k	k th eigenvector, ordered by highest eigenvalues
P	Eigenimages	t_1, t_2	Mask height and width
P_k	k th eigenimage	w	Number of wavelength channels in S
P_k^B	Mask-sized block in k th eigenimage	w^o	Number of wavelength channels in S^o
P^c	Subsampled eigenimages	$Z(i, j)$	Value of i th row and j th column (spatial surface) in matrix Z , where Z is any matrix with spatial dimensions.
P_k^c	k th subsampled eigenimage	$x_1, x_2,$	spatial indexes
		y_1, y_2	

Table II. Data sets.

Image set	Original sampling (nm)	Nr. of images	Contents
Misc ^a	5	7	Mixed collection of objects, including oil paint, Japanese paint, bottles, fruits, portrait, wool of different colors and an image of several colorful objects.
Cardboard ^b	10	18	Colorful cardboard packages of different products, e.g., packages of cereals, rice, tea, toothpaste, washing powder, etc.
Scenery ^c	10	6	Natural and urban images from the Minho region of Portugal.
Icons ^d	5	9	Various orthodox icons.
Printed ^d	5	24	Magazine papers, postcards and business cards printed with various printing devices.
Total		64	Total number of images.

^aReference 38.^bReference 39.^cReference 40.^dReference 33.

for the cardboard set with high color saturation, contrary to the scenery and icons sets. The icons set consists mostly of red and yellow colors, but also some small blue areas.

The light sources used are measured between 376 and 776 nm with a 2 nm interval. Spectral images and light sources spectra were interpolated to a 1 nm step with interpolation presented by Fairman.³⁶ The light source spectra

were then converted to between 400 and 700 nm by removing the wavelengths outside this range. After that, the spectral images were combined under the light source spectrum. The final data are then between 400 and 700 nm with a 1 nm sampling interval and defined as original data S^o . According to our previous study,¹² this interpolation phase does not generate a significant error in the results since the interpo-

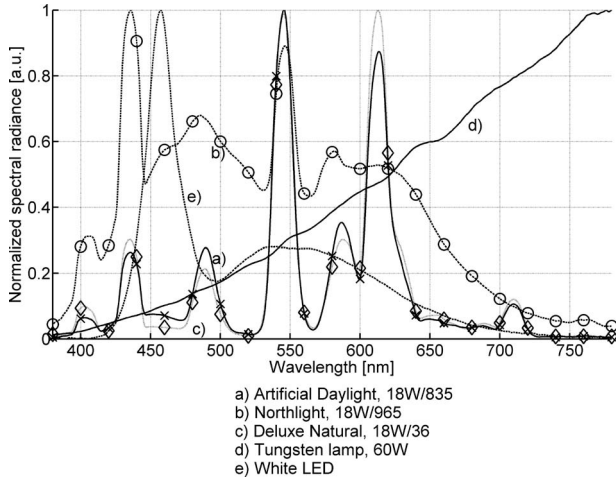
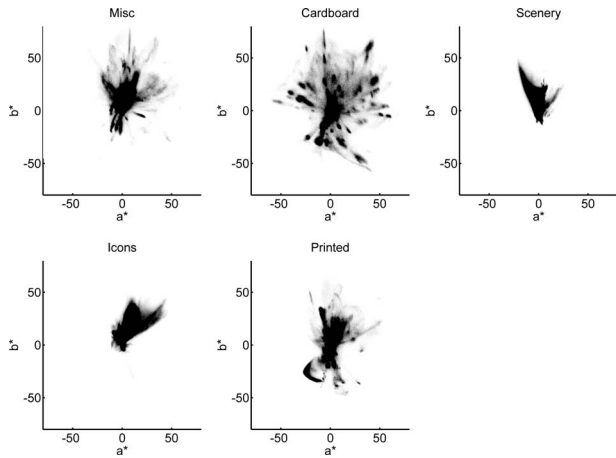


Figure 1. Spectra of real light sources.


 Figure 2. Color distribution of each set shown in (a^*, b^*) coordinate pairs projected from a CIE $L^*a^*b^*$ color space. The darker the point is in the coordination, the more pixels with same coordinate exist in the set.

lated reflectance spectra are very near to spectra measured with 1 nm interval. Similar results are also found by Sándor et al.⁴¹

EXPERIMENTS

Spatial Subsampling Masks

Typical mask matrixes based on JPEG-compression are called 4:4:4, 4:2:2, and 4:2:0 methods.³⁴ The corresponding masks for the spectral image compression used in this study are

$$\begin{aligned}
 B_k^{4:4:4} &= [1], \\
 B_k^{4:2:2} &= \begin{bmatrix} 1 & 0 \end{bmatrix}, \\
 B_k^{4:2:0} &= \begin{bmatrix} 1 & 0 \\ 0 & 0 \end{bmatrix}, \\
 \forall k &= 2, \dots, h.
 \end{aligned} \tag{10}$$

The same mask is used for eigenimages $P_2 - P_h$. In 4:4:4, there is no spatial subsampling since the mask dimensions

are 1×1 . In addition, three different 3×3 masks were used

$$\begin{aligned}
 B_k^{3 \times 3 \text{ center}} &= \begin{bmatrix} 0 & 0 & 0 \\ 0 & 1 & 0 \\ 0 & 0 & 0 \end{bmatrix}, \\
 B_k^{3 \times 3 \text{ average}} &= \begin{bmatrix} 1/9 & 1/9 & 1/9 \\ 1/9 & 1/9 & 1/9 \\ 1/9 & 1/9 & 1/9 \end{bmatrix}, \\
 B_k^{3 \times 3 \text{ median}} &= \begin{bmatrix} b_k^1 & b_k^2 & b_k^3 \\ b_k^4 & b_k^5 & b_k^6 \\ b_k^7 & b_k^8 & b_k^9 \end{bmatrix},
 \end{aligned}$$

$$b_k^i = \begin{cases} 1 & \text{for median pixel } b_k^i \hat{=} Md(P_k^B) \\ 0 & \text{otherwise,} \end{cases}$$

$$\forall k = 2, \dots, h, \tag{11}$$

where P_k^B is a corresponding 3×3 block from the k th eigenimage and $i = 1 - 9$. In the last median method, the mask is different in each eigenimage since the median value may be positioned differently in different eigenimages. In all other methods, the mask is the same for all eigenimages $P_2 - P_h$.

In the case where the image height or width is not divisible by the size of the mask, the eigenimages were temporally continued spatially with its mirror before subsampling, but only so much so that the size becomes divisible. For example, if the spatial size of an image is 301×299 and we use a 3×3 mask, one column needs to be added at the right edge of the eigenimage and two rows to the bottom edge to make the eigenimage size 303×300 . This is now divisible by the size of the mask. In this case, the last and second last rows are doubled to the bottom edge of the image in this order. The last column is then doubled to the right edge. These extra rows and columns were removed in the unsampling phase.

Quality and Error Limits

Average quality and error limits were chosen, which combined to give satisfactory results. As previously explained, $\Delta E < 1.0$ is not visually discernable and $GFC > 0.995$ is an accurate limit for spectra. These limits could also be used for spectral images of good quality, but spatial subsampling would not then be possible in any case. However, very accurate data may not be needed in the browsing phase. One may also think that the accuracy required in point color is not usually needed in spectral imaging. Unlike in point color measurements, spectral imaging may take a long time and therefore the risk of noise is higher. In addition, color quality is not usually required in such accuracy as in point spectra. When a spectrum is located in a huge spectral image, the observer does not see just one color of a certain pixel, but

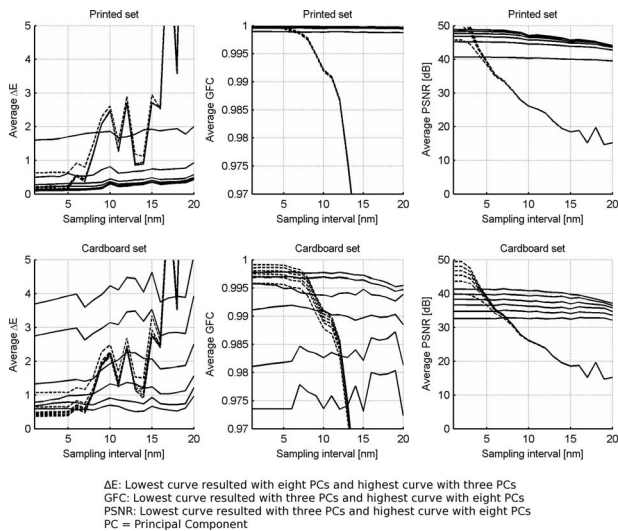


Figure 3. Average ΔE , GFC, and PSNR values for reflectance data (solid) and data under artificial daylight (dashed) in the printed and cardboard image set with a mask 4:4:4 and with 3-8 principal components (curves).

also all other pixels in the image. The surrounding pixels give an effect to the visualization, and so, the color of one pixel cannot be seen accurately. Therefore, the less strict threshold limits were chosen, as average PSNR > 30 dB, average GFC > 0.99 and average ΔE < 3.0. The limit ΔE < 3.0 for spectral images was also recommended by Zhang and Wandell,⁴² and the limit GFC \geq 0.99 was defined as acceptable by Romero et al.⁴³ with different natural and artificial illuminants. The chosen quality and error limits correlate depending on the used light source. For example, with data under an F2 illuminant, all quality and error measures result in the same selections. For data under artificial daylight, ΔE < 3.0 is gained very easily, but PSNR and GFC limit the selections most. For data under D65 illuminant, the major limiter for the selections is the ΔE measure. Generally, the correspondence of the limits used is a compromise with the light sources used.

However, with increasing sampling interval, oscillation of the error and quality values may occur with wide sampling intervals, especially for the data under peaky light sources, because with some sampling intervals the peaks are caught and with others they are missed. To avoid this issue, it is necessary that the quality and error limits must also be established with all the more accurate sampling intervals and higher number of principal components than the chosen ones. With subsampling, it is possible to choose a mask of smaller size than the selected one. If the selected replacement pixel is one selected pixel from the block, then an average or median pixel can also be used. Similarly, a median pixel can be used instead of an average pixel.

Evaluation of Quality and Error Measures

Let us first concentrate on the reflectance data and on the data under an artificial daylight source. The average ΔE error and average PSNR and GFC quality values of the printed and cardboard sets are shown in Figure 3. Here, sampling intervals of 1 and 20 nm are used, which is shown in the

horizontal axis. The data are compressed with 3–8 principal components. No subsampling is used. The quality of the reconstructed spectra with a different number of principal components is shown as different curves in the image. The solid curves are generated with reflectance data and dashed curves with data under an artificial daylight source. In GFC and PSNR calculations, the lowest curve corresponds to compression with three principal components, and in the higher curves more principal components are used. Likewise, in ΔE calculations, the highest curve corresponds to compression with three principal components, and in the lower curves more principal components are used. The results are very different between these two sets. The curves in the printed set are practically stacked together. On the contrary, with the cardboard reflectance set, the curves are different with a different number of principal components, but again stacked together in the set under the light source. The ΔE errors for the reflectance data of the printed set show that all used sampling intervals give good results, especially if four or more principal components are used. GFC and PSNR give good results with any sampling interval and with any number of principal components used. In the case of the cardboard set, five, six, and three principal components are required for ΔE , GFC, and PSNR limits, respectively, for any sampling interval. Therefore, because of the GFC limit, six principal components should be chosen. For the printed data under the artificial daylight source, a 16 nm interval with three principal components is enough with the ΔE error. If using a GFC measure, an 11 nm interval with three principal components is enough. In the case of PSNR, 8 nm sampling with three principal components is required. The quality is a lot poorer with wider sampling intervals. For the cardboard data under the artificial daylight source, GFC and PSNR values are above the limits with 8 nm and 9 nm intervals, respectively, with three principal components. With the ΔE limit, an interval as wide as 14 nm could be used, but now PSNR and GFC measures limit the selections.

The subsampling phase gives a high negative effect for the errors, which is shown in Figure 4. It can be also seen that a 3×3 mask gives similar results to a 4:2:0 mask, with the exception of the ΔE error. Here, the printed set (unplotted curves) and the cardboard set (plotted curves) with eight principal components and a 5 nm sampling interval were used. The dashed curves are created from data under an artificial daylight source and solid curves from data from reflectance spectral images.

Procedure for Selecting the Parameters

A suitable sampling interval and number of principal components, which satisfy the quality and error limits, were chosen for each subsampling mask and for each image set separately, by using average quality and error measures from each image. The selection process can be done in several ways, resulting in different combinations of sampling interval, number of principal components, and subsampling mask; but the method shown in Figure 5 was used. At first, for each image in a set, the widest possible sampling interval with the required number of principal components was cal-

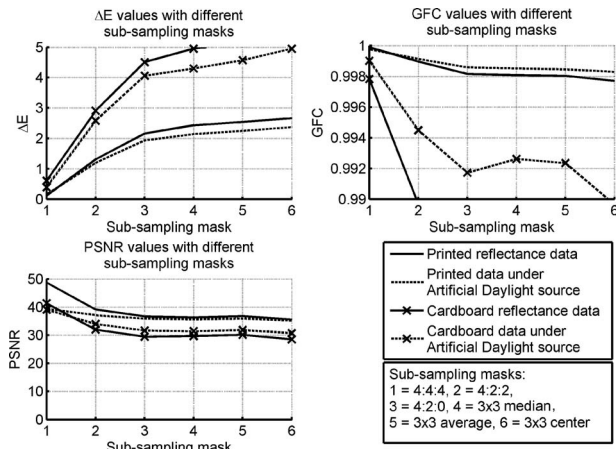


Figure 4. Average ΔE , GFC, and PSNR values for reflectance data (solid) and data under an artificial daylight (dashed) in the printed (unplotted) and the cardboard (plotted) image sets with a 5 nm sampling, eight principal components, and different subsampling masks.

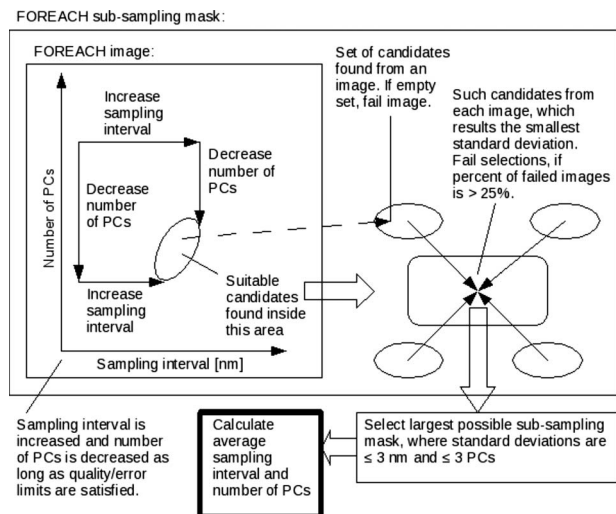


Figure 5. Selection procedure.

culated. Then, the lowest number of principal components with the required sampling interval was calculated. These selections were set as the lower and upper boundaries for the final selections of sampling interval and principal components. In this boundary search, all narrower sampling intervals and higher number of principal components must also satisfy the results. After this, all possible combinations were found between these boundaries. For each image, such final selections were found where the standard deviations of sampling intervals and number of principal components between the images are the smallest. This was done with each spatial subsampling mask and image set separately. However, it was found that with some subsampling masks, few images of some data sets under some light sources failed to achieve the quality and error limits for any number of principal components below 20. Therefore, only such combinations were considered as candidates, where over 75% of the images satisfy the error and quality limits and, if possible, standard deviations of selected sampling intervals and numbers of principal components are less than 3 nm and three compo-

nents, respectively. Next, such selections for each image were found from the candidates, which cause the smallest standard deviations with the largest possible subsampling mask. The final selections for the whole data set are the averages of these selections. With these conditions, the quality and error values of the failed images are also close to the limits, and the overall results remain acceptable.

RESULTS

The final chosen sampling intervals, number of principal components, and subsampling masks for each data set are shown in Figure 6. Each ellipse is created with the data set under certain light source. The central point of an ellipse shows the average selected sampling interval and number of principal components for the data set. The ellipse denotes the standard deviations of the sampling intervals and principal components selected for each image in the set. The color of the ellipse shows the spatial subsampling mask used. The text on the side of the ellipse denotes the light source used and relative number of images in a set used in the selection procedure. Almost all ellipses are small in the chosen selections, which means that the selections of different images are, in general, close to average selections.

Generally, a 20 nm sampling interval is enough for reflectance data and data under such light sources, whose spectrum is smooth. The cardboard and scenery sets require five or six and four or five principal components, respectively. With the icons set, data under a tungsten light source and illuminant A also require six principal components. All other reflectance data sets or data sets under a smooth light source require four principal components. Mask 4:4:4 must be used for the cardboard sets and also for the scenery data under illuminant A. Mask 4:2:2 is needed for reflectance data and data under illuminant D65 in the misc and icons sets. Mask 4:2:0 was selected for the scenery data under a tungsten light source. Mask size 3 × 3 is enough for all the other reflectance sets and sets under smooth light sources. In the icons set under a tungsten light source or illuminant A, high subsampling creates high error, which is compensated with a high number of principal components. With the reflectance cardboard data and the same data under smooth light sources, subsampling does not work at all.

For the data under an artificial daylight or deluxe natural light source, a 6–9 nm interval with 3–5 principal components are required. With different data sets under a Northlight source, a 10–16 nm interval with 3–4 principal components are needed, with the exception of the cardboard set, where 4:2:2 subsampling causes a high error requiring eight principal components with an 8 nm sampling interval. The selected sampling interval and number of principal components for data under a white LED light is similar to selections for data under a Northlight source. Generally, a 4:2:2 mask can be used for the cardboard data under different real fluorescent light sources. Depending on the peaky light source, a 4:2:2 or 4:2:0 mask is required for the misc and icons sets. For the scenery and printed set, a 3 × 3 average mask can be used, generally. However, some exceptions are found, for example, masks 4:2:0 and 4:2:2 are required in

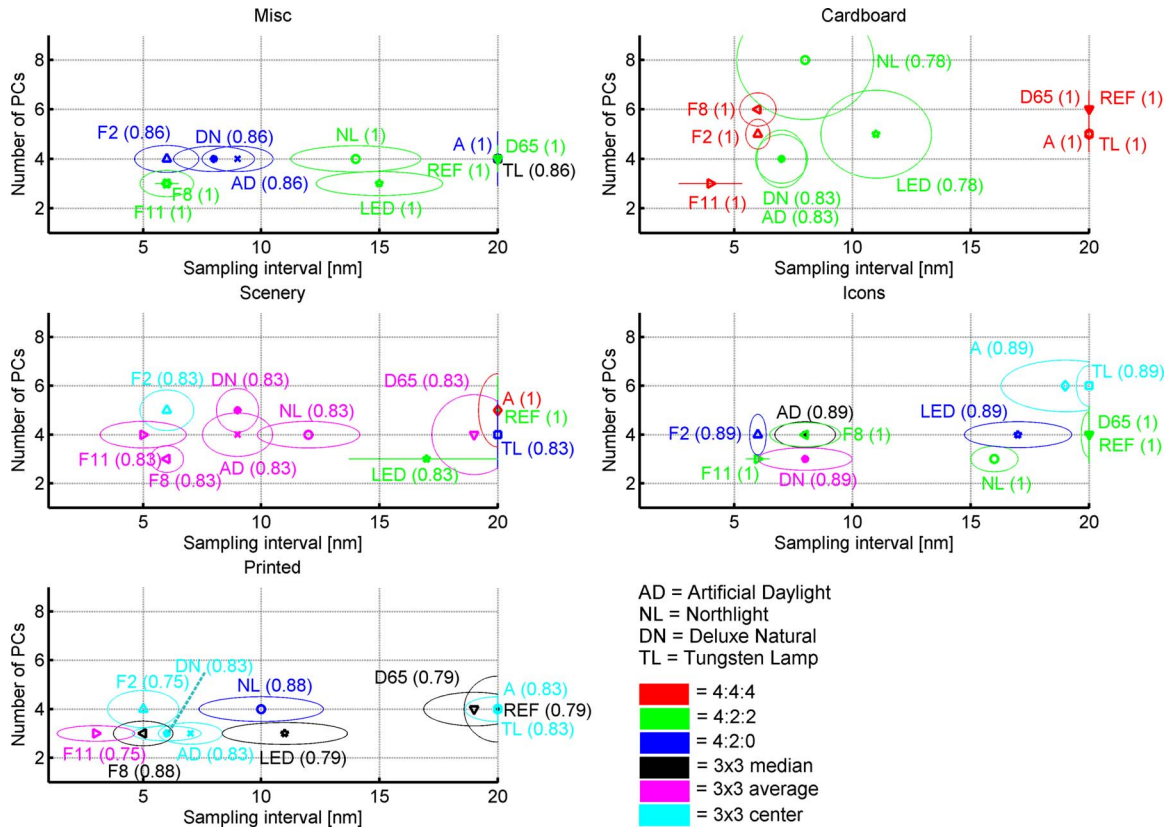


Figure 6. Optimal average selections for different data sets under different light sources. Ellipses represent the standard deviation of selections done for each image separately.

the printed set with a Northlight source and in the scenery set with a white LED source.

For F illuminants, a 3–6 nm sampling interval with 3–6 principal components are needed with different sets. In addition, mask 4:2:2 or 4:2:0 can be used for the misc and icons sets. Mask 4:4:4 is required for the cardboard set, but a 3 × 3 mask is possible with the scenery and printed sets. The replacement pixel can be a center pixel with an F2 illuminant, but must be a median pixel for the printed set under F8 illuminant, and an average (or median) pixel with other F illuminants.

Some average errors for all images in the printed and cardboard reflectance sets and sets under an artificial daylight source are found in Table III. For reflectance data sets, the errors are clearly smaller than the limits, so a sampling interval wider than 20 nm would also be accepted. However, with the cardboard set under an artificial light source, the ΔE and PSNR results are close to the error and quality limits, and with the printed set under an artificial daylight source, the GFC and PSNR results are close to the quality limits. The compression ratio is calculated between the uncompressed data with a selected sampling interval and

Table III. Optimal average selections and results of the cardboard and printed reflectance data sets and data sets under artificial daylight.

Image set	Reflectance		Artificial daylight		
	Selections	Quality/Error	Average		
Cardboard	20 nm,	ΔE 1.6	7 nm,	ΔE 2.8	
	6 PCs,	GFC 0.994	4 PCs,	GFC 0.993	
	4:4:4,	PSNR 35.9	4:2:2,	PSNR 31.4	
	CR ^a : 3:1		CR ^a : 18:1		
Printed	20 nm,	ΔE 2.7	7 nm,	ΔE 2.6	
	4 PCs,	GFC 0.998	3 PCs,	GFC 0.997	
	3 × 3 median,	PSNR 35.7	3 × 3 center,	PSNR 31.9	
	CR ^a : 12:1		CR ^a : 36:1		

^aCompression ratio.

Table IV. Compression ratios of an image measured between 400–700 nm.

Sampling interval of uncompressed image	5 nm	10 nm	20 nm
4 PCA, 4:4:4	15:1	8:1	4:1
4 PCA, 4:2:0	35:1	18:1	9:1
4 PCA, 3 × 3	46:1	23:1	12:1
6 PCA, 4:4:4	10:1	5:1	3:1
6 PCA, 4:2:0	27:1	14:1	7:1
6 PCA, 3 × 3	39:1	20:1	10:1
8 PCA, 4:4:4	8:1	4:1	2:1
8 PCA, 4:2:0	22:1	11:1	6:1
8 PCA, 3 × 3	34:1	17:1	9:1

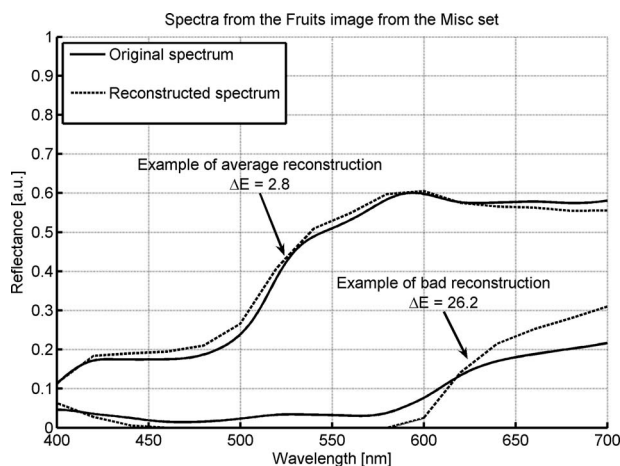


Figure 7. Average and bad cases of a reconstructed spectrum. In compression, 20 nm sampling, four principal components, and a 4:2:0 mask matrix were used.

compressed data with a selected number of principal components and subsampling mask. Different examples of compression ratios for the method are shown in Table IV. In these examples, the compression ratio varies between 2:1-12:1, 4:1-23:1, and 8:1-46:1 with a 20 nm, 10 nm, and 5 nm sampling interval of the uncompressed image, respectively. An average and bad case example of spectrum reconstruction can be found in Figure 7, when four principal components and a 4:2:0 subsampling mask was used.

DISCUSSION

The results fall into three groups: reflectance data and data under smooth light sources, data under real fluorescent light sources, and data under standard F illuminants. The light source has a very high effect on the sampling interval. For reflectance data and data under smooth light sources, 20 nm is enough. For real fluorescent light sources, 6–9 nm is required, with the exception of the smoother light sources Northlight and white LED, where a wider sampling interval between 10 and 17 nm can be used. With these light sources, the subsampling mask used affects the sampling interval: a larger mask requires a more accurate sampling interval. This compensates for the error generated in subsampling. The

required sampling interval is most accurate for the data under F illuminants, with 3–6 nm. In the printed set, the four CMYK primaries between different printers are similar and, therefore, the required number of principal components is also low, between three and four. On the other hand, there are various strong colors in the cardboard set, creating a need for several principal components. The items in the misc and in the scenery sets are more common targets for spectral imaging, and four or five principal components are required. In general, the results of all sets fall between four and six principal components. While the peaks of a peaky light source require an accurate sampling interval, the light source spectrum converts the spectra more similar to each other, which may require less principal components in some cases than with reflectance spectra, e.g., in the scenery set. Since the spectra are similar, the overall dimensionality is smaller. Stacking, shown in Fig. 3, occurs, and adding more principal components does not develop the data at all.

It is usual that spectral measurements are done with a 10 nm sampling interval. But in the measuring phase, one should be careful in choosing the sampling interval. This study, among others,^{12,13} shows that a 10 nm sampling interval is not enough for fluorescent light sources. This question will become more and more important due to the increasing popularity of fluorescent and LED based light sources.

Subsampling is highly dependent on the data set and light source and, practically, it does not work with the cardboard set. The product packages include a lot of sharp edges between totally different color hues. These edges made it impossible to use subsampling since the color edge would clearly change after subsampling. However, if the data set contains images with weak color edges or the edges are not important, subsampling can be used even up to a 3 × 3 mask. In general, a 3 × 3 mask can well be used with sets similar to the printed or scenery sets, but 4:2:0 and 4:2:2 is good with the icons and misc data. In the icons and misc set, sharp color edges also exist, but not with as strong a color change as in the cardboard set.

The ΔE and PSNR results with the reflectance data sets are very similar to the results in the study of Hauta-Kasari et al.²³ with the Coral database.⁴⁴ If the quality and error limits are used, three principal components and a 4:2:0 mask seem to not be acceptable for the Coral database nor for the reflectance data sets used in this study. Similar PSNR values as in Table III were also arrived at by Chang²⁸ and Chang et al.³⁰ The resulting compression ratios are also generally similar to other compression methods given in the introduction section. A small practical test was done and repeated five times with an Intel Pentium 4 HT 2.4GHz CPU and with 2 × 512 MB of memory. Downloading an uncompressed image required an average 78.3 s with a broadband 4 Mbit ADSL connection. However, downloading the compressed image required only 3.4 s, including reconstruction time with MATLAB software. Here the original image was measured with a 5 nm sampling interval. The compression was done with five principal components and a 4:2:0

subsampling mask. Because of the simplicity of the subsampling, the spatial reconstruction requires minimal processor time. In addition, spatial subsampling required only 0.2 s with MATLAB software, which makes it possible for the user to choose the subsampling mask that is applied to the spectral image before transmission.

CONCLUSIONS

A suitable sampling interval, number of principal components, and spatial subsampling mask were found for a spectral image browsing method, with different spectral image sets under various light sources and standard illuminants. It was shown that even a 20 nm sampling interval is enough for spectral imaging under smooth light sources. However, 10 nm is not enough for spectral imaging under peaky light sources. A suitable number for principal components was found to range between four and six. Spatial subsampling affects the image quality, but for browsing purposes, a mask of up to 3×3 can be used.

REFERENCES

- ¹W. Thornton, "How strong metamerism disturbs color spaces", *Color Res. Appl.* **23**, 402–407 (1998).
- ²P. Morovic, "Metamer sets", Ph.D. dissertation, University of East Anglia, Norwich, 2002.
- ³M. Nishibori, "Problems and solutions in medical color imaging", *Proc. 2nd Int. Symp. on Multispectral Imaging and High Accurate Color Reproduction* (Chiba University, Chiba, Japan, 2002) pp. 9–17.
- ⁴T. Hyvärinen, E. Herrala, and A. Dall'Avà, "Direct sight imaging spectrograph: A unique add-on component brings spectral imaging to industrial applications", *Proc. SPIE* **3302**, 165–175 (1998).
- ⁵K. Martinez, J. Cupitt, D. Saunders, and R. Pillay, "Ten years of art imaging research", *Proc. IEEE* **90**, 28–41 (2002).
- ⁶H. Motomura, N. Ohya, M. Yamaguchi, H. Haneishi, K. Kanamori, and S. Sannohe, "Development of six-primary HDTV-display system", *Proc. 22nd Int. Display Research Conf., Eurodisplay 2002* (Society for Information Display, Campbell, CA, 2002) pp. 563–566.
- ⁷K. Ohsawa, T. Ajito, Y. Komiyama, H. Haneishi, M. Yamaguchi, and N. Ohya, "Six-band HDTV camera system for spectrum-based color reproduction", *J. Imaging Sci. Technol.* **48**, 85–92 (2004).
- ⁸F. Imai, M. Rosen, D. Wyble, R. Berns, and D. Tzeng, "Spectral reproduction from scene to hardcopy I: Input and output", *Proc. SPIE* **4306**, 346–357 (2001).
- ⁹J. Hallikainen, J. Parkkinen, and T. Jaaskelainen, "Color image processing with AOTF", *Proc. of 6th Scandinavian Conf. on Image Analysis* (Pattern Recognition Society of Finland, Oulu, Finland, 1989) pp. 294–300.
- ¹⁰S. Tominaga, "Spectral imaging by a multichannel camera", *J. Electron. Imaging* **8**, 332–341 (1999).
- ¹¹K. Itoh, in *Progress in Optics XXXV*, edited by E. Wolf (Elsevier Science, Amsterdam, 1996), pp. 145–196.
- ¹²J. Lehtonen, J. Parkkinen, and T. Jaaskelainen, "Optimal sampling of color spectra", *J. Opt. Soc. Am. A Opt. Image Sci. Vis* **23**, 2983–2988 (2006).
- ¹³H. Trusselli and S. Kulkarni, "Sampling and processing of color signals", *IEEE Trans. Image Process.* **5**, 677–681 (1996).
- ¹⁴T. Keusen and W. Praefcke, "Multispectral color system with an encoding format compatible to the conventional tristimulus model", *Proc. IS&T/SID 3rd Color Imaging Conf.* (IS&T, Springfield, VA, 1995).
- ¹⁵G. Canta and G. Poggi, "Compression of multispectral images by address-predictive vector quantization", *Signal Process. Image Commun.* **11**, 147–159 (1997).
- ¹⁶A. Hyvärinen, J. Karhunen, and E. Oja, *Independent Component Analysis* (Wiley, New York, 2001).
- ¹⁷T. Wachtler, T.-W. Lee, and T. Sejnowski, "Chromatic structure of natural scenes", *J. Opt. Soc. Am. A Opt. Image Sci. Vis* **18**, 65–77 (2001).
- ¹⁸J. Parkkinen, J. Hallikainen, and T. Jaaskelainen, "Characteristic spectra of Munsell colors", *J. Opt. Soc. Am. A* **6**, 318–322 (1989).
- ¹⁹D. Tzeng and R. Berns, "A review of principal component analysis and its applications to color technology", *Color Res. Appl.* **30**, 84–98 (2005).
- ²⁰A. Mansouri, T. Sliwa, J. Hardeberg, and Y. Voisin, "Representation and estimation of spectral reflectances using projection on pca and wavelet bases", *Color Res. Appl.* **33**, 485–493 (2008).
- ²¹P. Carmona and R. Lenz, "Performance evaluation of dimensionality reduction techniques for multispectral images", *Int. J. Imaging Syst. Technol.* **17**, 202–217 (2007).
- ²²S. Lim, K. H. Sohn, and C. Lee, "Principal component analysis for compression of hyperspectral images", *Proc. International Geoscience and Remote Sensing Symposium* (IEEE, Piscataway, NJ, 2001) pp. 97–99.
- ²³M. Hauta-Kasari, J. Lehtonen, J. Parkkinen, and T. Jaaskelainen, "Image format for spectral image browsing", *J. Imaging Sci. Technol.* **50**, 572–582 (2006).
- ²⁴J. Saghri, A. Tescher, and J. Reagan, "Practical transform coding of multispectral imagery", *IEEE Signal Process. Mag.* **12**, 32–43 (1995).
- ²⁵A. Kaarna, "Multispectral image compression using the wavelet transform", Ph.D. dissertation, Lappeenranta University of Technology, Lappeenranta, Finland, 2000.
- ²⁶Q. Du and J. Fowler, "Hyperspectral image compression using JPEG2000 and principal component analysis", *IEEE Geosci. Remote Sens.* **4**, 201–205 (2007).
- ²⁷R. Kumar and V. Makkapati, "Encoding of multispectral and hyperspectral image data using wavelet transform and gain shape vector quantization", *Image Vis. Comput.* **23**, 721–729 (2005).
- ²⁸L. Chang, "Multispectral image compression using eigenregion-based segmentation", *Int. J. Pattern Recognit. Artif. Intell.* **37**, 1233–1243 (2004).
- ²⁹Y. Zhang and D. Desai, "Hyperspectral image compression based on adaptive recursive bidirection prediction/JPEG", *Int. J. Pattern Recognit. Artif. Intell.* **33**, 1851–1861 (2000).
- ³⁰L. Chang, C.-M. Cheng, and T.-C. Chen, "An efficient adaptive KLT for multispectral image compression", *Proc. 4th IEEE Southwest Symposium on Image Analysis and Interpretation* (IEEE, Piscataway, NJ, 2000) pp. 252–255.
- ³¹G. Ubierno, "Lossless region-based multispectral image compression", *Proc. of 6th Int. Conf. on Image Processing and Its Applications* (IEEE, Piscataway, NJ, 1997) pp. 64–68.
- ³²A. Kaarna, "Integer PCA and wavelet transforms for multispectral image compression", *Proc. International Geoscience and Remote Sensing Symposium* (IEEE, Piscataway, NJ, 2001) pp. 1853–1855.
- ³³"Spectral database", University of Joensuu Color Group, <http://spectral.joensuu.fi/> (accessed Oct. 19, 2008).
- ³⁴C.-H. Wu and J. Irwin, *Emerging Multimedia Computer Communication Technologies* (Prentice-Hall, Englewood Cliffs, NJ, 1998).
- ³⁵N. Ohta and A. Robertson, *Colorimetry Fundamentals and Applications* (Wiley, New York, 2005).
- ³⁶H. Fairman, "The calculation of weight factors for tristimulus integration", *Color Res. Appl.* **10**, 199–203 (1985).
- ³⁷J. Hernández-Andrés, J. Romero, and R. Lee, Jr., "Colorimetric and spectroradiometric characteristics of narrow-field-of-view clear skylight in Granada, Spain", *J. Opt. Soc. Am. A Opt. Image Sci. Vis* **18**, 412–420 (2001).
- ³⁸O. Kohonen, M. Hauta-Kasari, K. Miyazawa, J. Parkkinen, and T. Jaaskelainen, "Organizing spectral image database using self-organizing maps", *J. Imaging Sci. Technol.* **49**, 431–441 (2005).
- ³⁹G. Finlayson, S. Hordley, and P. Morovic, "Using the spectracube to build a multispectral image database", *Proc. of the 2nd European Conf. on Colour in Graphics, Imaging and Vision* (IS&T, Springfield, VA, 2004) pp. 268–273.
- ⁴⁰S. Nascimento, F. Ferreira, and D. Foster, "Statistics of spatial cone-excitation ratios in natural scenes", *J. Opt. Soc. Am. A Opt. Image Sci. Vis* **19**, 1484–1490 (2002).
- ⁴¹N. Sándor, T. Ondró, and J. Schanda, "Spectral interpolation errors", *Color Res. Appl.* **30**, 348–353 (2005).
- ⁴²X. Zhang and B. Wandell, "A spatial extension of CIELAB for digital color image reproduction", *Proc. SID* **5**, 61–63 (1997).
- ⁴³J. Romero, A. García-Beltrán, and J. Hernández-Andrés, "Linear bases for representation of natural and artificial illuminants", *J. Opt. Soc. Am. A Opt. Image Sci. Vis* **14**, 1007–1014 (1997).
- ⁴⁴C.-C. Chiao, T. Cronin, and D. Osorio, "Color signals in natural scenes: Characteristics of reflectance spectra and effects of natural illuminants", *J. Opt. Soc. Am. A Opt. Image Sci. Vis* **17**, 218–224 (2000).